Supplementary Material (ESI) for Journal of Materials Chemistry

[Supplementary Information]

Direct Growth of β-$FeSi_2$ Nanowires with Infrared Emission, Ferromagnetism at Room Temperature and High Magnetoresistance via a Spontaneous Chemical Reaction Method

Shih-Wei Hung,[a] Ping-Hung Yeh,[b] Li-Wei Chu,[a] Chii-Dong Chen,[c] Li-Jen Chou,[a] Yi-Jen Wu[a], and Lih-Juann Chen[a*]

[a]*Department of Material Science and Engineering, National Tsing Hua University, Hsinchu, Taiwan, ROC.*

Fax: +886-3-5718328; Tel: +886-3-5731166; E-mail: ljchen@mx.nthu.edu.tw

[b]*Department of Physics,Tamkang University,Tansui,Taiwan 251, R. O. C*

[c] *Institute of Physics, Academia Sinica, Taipei, Taiwan, R. O. C.*

Supporting Information S1. The nanostructures formed at regions A, B, C, and D in the furnace with the DS heating zone set at 800 ℃ and Ar + 20 % H_2 flow rate maintained at 150 SCCM.

Figure S1(a) shows the experimental setup of the spontaneous chemical vapor transport growth system. Figure S1(b) shows the reaction products found in region A. The samples near the precursors encountered very high vapor flux and porous structures were obtained as a result of the reaction of large amount of precursor vapor with the Si substrate.

The optimum synthesis condition for β-$FeSi_2$ nanowires was realized with the heating zone DS set at 800 ℃. For Si substrates placed in regions B and C, sheet structure and a high density of 30 to 60 μm β-$FeSi_2$ nanowires were formed, respectively. The nanowires were favored to grow at appropriate flux condition. 1 to 3 μm nanowires were found in region D compared to those in region C. An example is shown in Fig.

S1(e). In this region, vapor flux is relatively low to grow long nanowires.

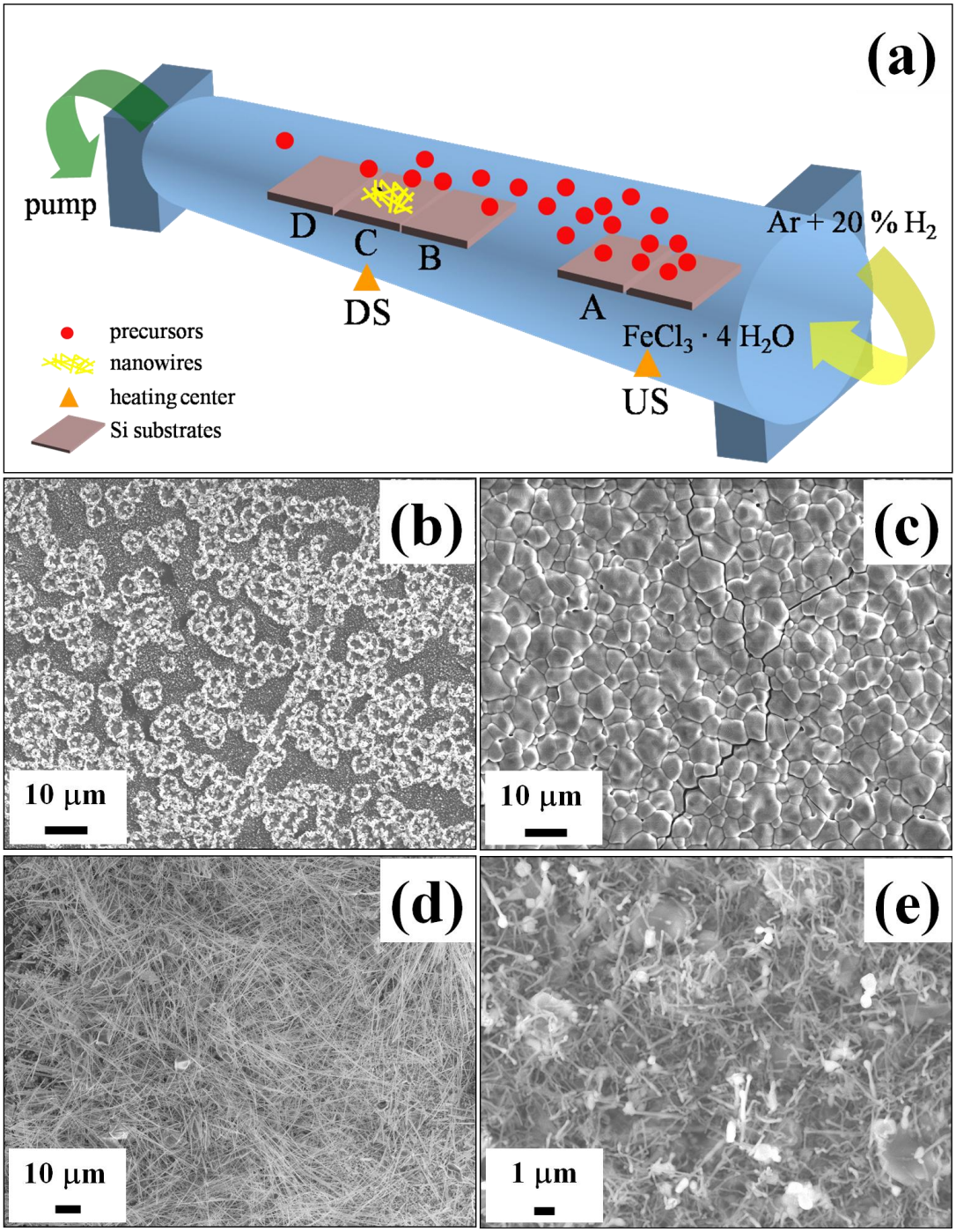

Fig. S1 (a) Experimental setup of the spontaneous chemical vapor transport growth system. (b), (c), (d), and (e) are SEM images of the products grown at region A, B, C and D, respectively.

Supporting Information S2. The nanostructures formed at regions C in the furnace

with the DS heating zone set at 650, 900, and 1000 ℃.

Figures S2(a) and (b) show SEM images of the reaction products formed in region C at the DS zone temperature of 900 and 1000℃, respectively. Only micrometer-sized particles were found in these two samples. Particle size was increased from 5 to 8 μm when the growth temperature was increased from 900 to 1000℃, respectively. On the other hand, FeSi nanowires can be observed when DS zone temperature was lowered to 650 ℃. An SEM image is shown in Fig. S2(c). Analysis of XRD spectra indicates that all diffractions peaks can be ascribed to the FeSi phase with a cubic structure, as shown in Fig. S2(d). Thermodynamically, FeSi is favored to grow at low temperature compared to β-$FeSi_2$, and the activation energy for FeSi and β-$FeSi_2$ was calculated to be 1.36 and 1.5 eV, respectively.[3] Apparently, the growth of β-$FeSi_2$ nanowires was influenced by growth temperature and a variation in vapor flux with the location in the furnace significantly. By controlling the vapor flux of the precursors and the heating temperature of the substrates, we can obtain a high density of β-$FeSi_2$ nanowires with core shell structures.

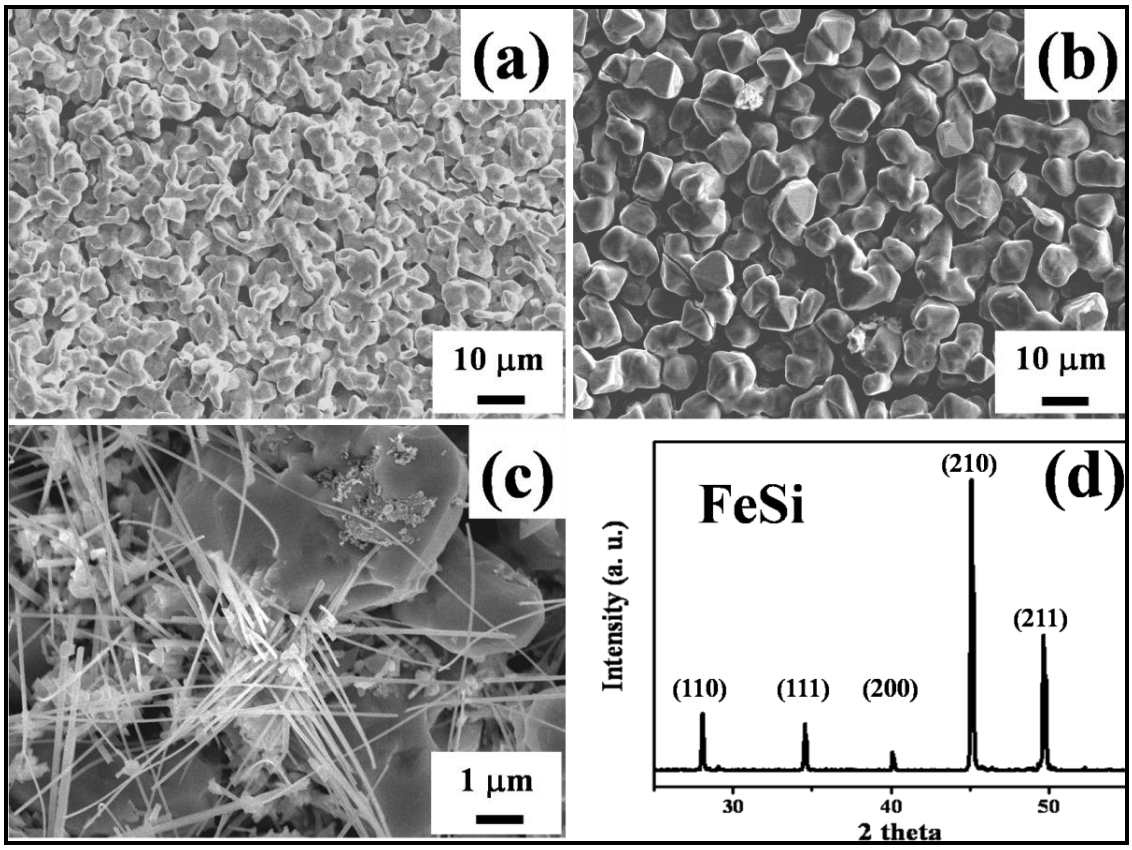

Fig. S2(a), (b), and (c) show the SEM images of the reaction products found in region C at the DS zone growth temperature of 900, 1000 and 600 ℃, respectively. (d) XRD spectrum confirms that the nanowire is FeSi phase with a cubic structure.

Supporting Information S3. Characterization of core shell β-$FeSi_2$ nanowires grown in region D.

Fig. S3(a) shows the low-magnification TEM image of an individual β-$FeSi_2$ nanowire with a 25-70 nm core and 20-35 nm shell grown in region D. The surface of the nanowire is not as smooth as nanowires grown in region C. The inset shows the SAED pattern obtained from a representative nanowire, which can be indexed to an orthorhombic β-$FeSi_2$ structure (a=0.9863 nm, b=0.7791 nm and c=0.7833 nm). To confirm the chemical compositions of the core shell β-$FeSi_2$ nanowire, EDS spectrum taken from the shell is composed of Si and O, as illustrated in Fig. S2(b). No Fe or other impurities were found in shell layer. EDS spectrum taken from the core layer is composed of Fe and Si with an atomic ratio close to 1:2, as shown in Fig. S2(c). Fig. S2(d) reveals the high-magnification TEM image of a β-$FeSi_2$ nanowire. The corresponding high-resolution TEM (HRTEM) image is shown in the inset and clearly presents the single-crystalline structure of the nanowire, without liner or planar defects. The two d-spacings of 0.39 nm and 0.495 nm were identified as β-$FeSi_2$ (002) and (200) planes, respectively.

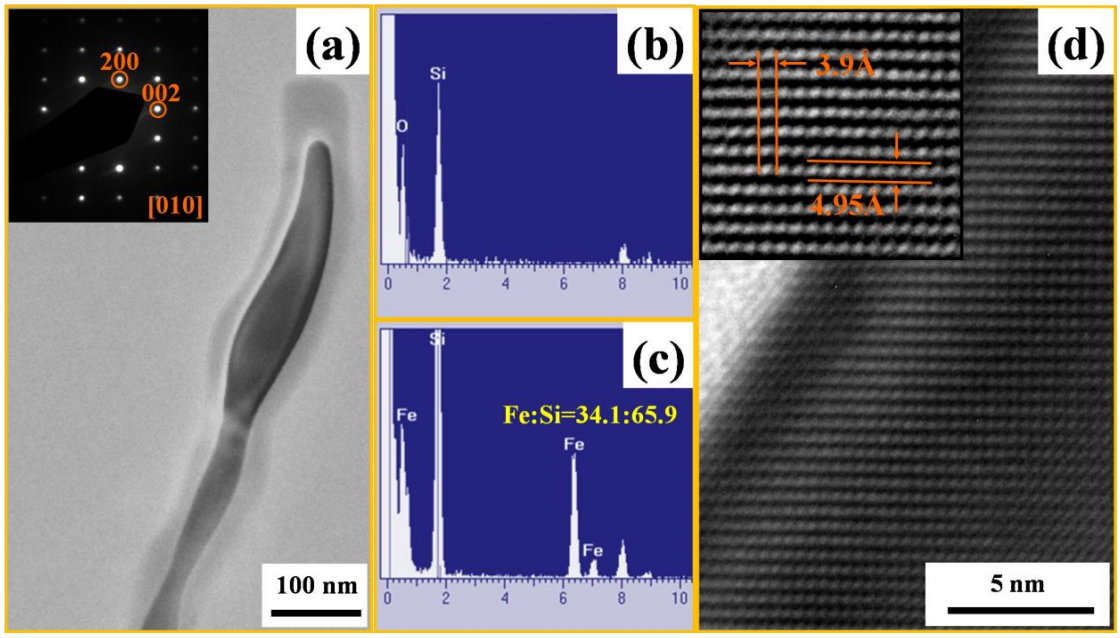

Fig. S3 Representative TEM analyses of the core shell β-$FeSi_2$ nanowires: (a) low-magnification image of a nanowire with core-shell structure. Inset: SAED pattern indicating that the β-$FeSi_2$ is single-crystalline, (b) EDS spectrum shows the shell layer is composed of Si and O, (c) EDS analysis shows chemical compositions of Fe:Si is close to 1:2, and (d) high-magnification image of a β-$FeSi_2$ nanowire. Inset: HRTEM image confirming that the nanowire is β-$FeSi_2$.

Supporting Information S4. In our EDS analyses shown in Fig. S2(b) and Fig. S(b), shell layer of β-$FeSi_2$ nanowires contains only Si and O. No Fe or other impurities were found. To obtain the intrinsic properties of the as-grown β-$FeSi_2$ nanowire, samples for magnetic properties measurement will be performed after dipping with dilute HF (3 wt. %) for 10 s to remove the silicon oxide layer.

Supporting Information S5. Flow chart of the nanodevice fabrication for magnetoresistance measurement.

Fig. S5 shows the flow chart of the nanodevice fabrication processes. Samples for magnetoresistance measurement will be performed after dipping with dilute HF (3 wt. %) for 10 s to remove the silicon oxide layer. Furthermore, to obtain an oxide free surface between nanowire and metal electrode, plasma etching for 30 s is conducive to cleaning nanowire surface.

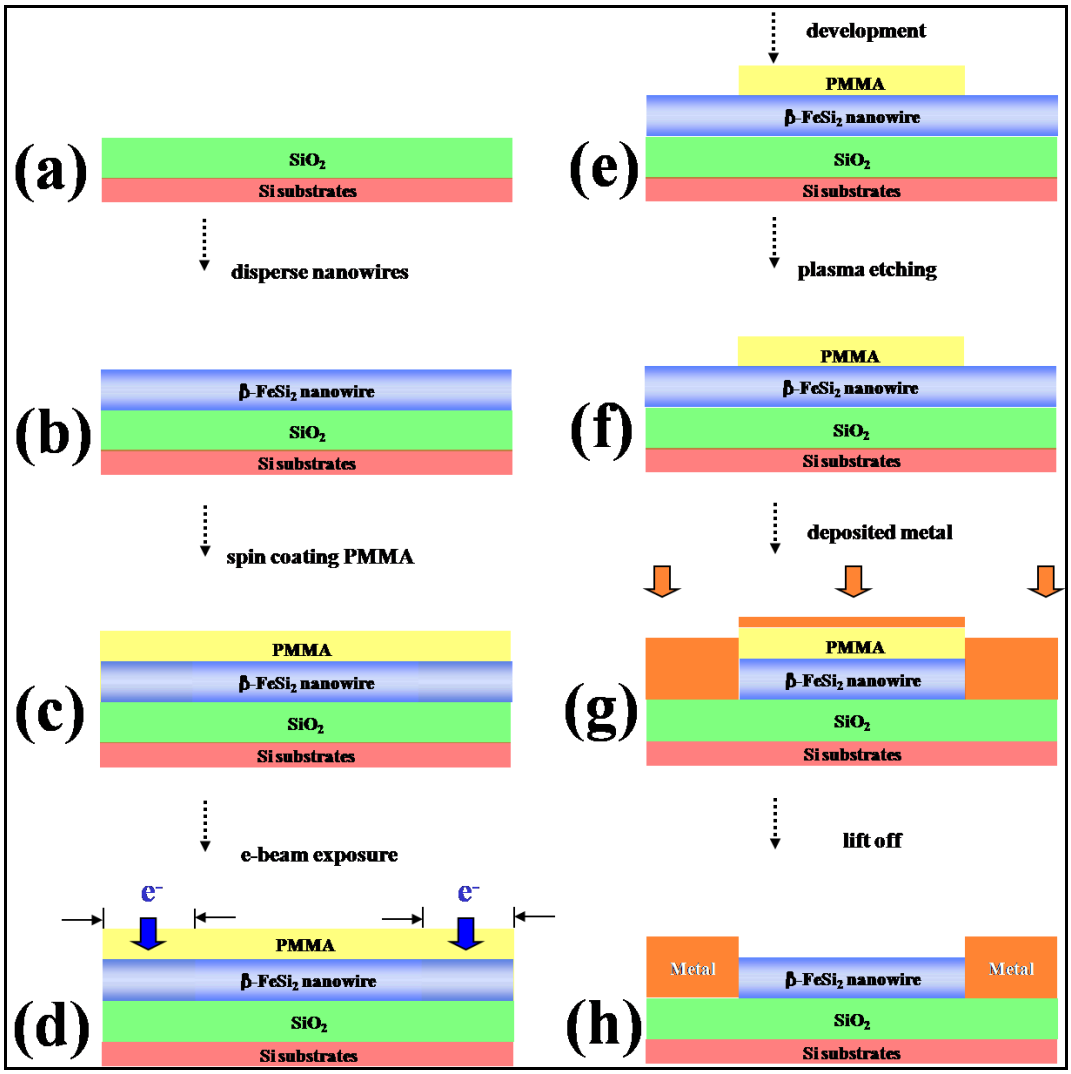

Fig. S5 Flow chart of the β-$FeSi_2$ nanodevice fabricated with standard e-beam lithography processes for MR measurement.

References

1 C. A. Dimitriadis and J. H. Werner, *J. Appl. Phys.*, 1990, **68**, 93.

2 K. Radermacher, S. Mantl, C. Dieker, H. Lüth and C. Freiburg, *Thin Solid Film*, 1992, **215**, 76.

3 N. R. Baldwin and D. G. Ivey, *J. Mater. Sci.*, 1996, **31**, 31.